Pharm Res (2010) 27:2221–2233
DOI 10.1007/s11095-010-0228-1

RESEARCH PAPER

Anisotropic Porous Structure of Pharmaceutical Compacts Evaluated by PGSTE-NMR in Relation to Mechanical Property Anisotropy

Patrice Porion • Virginie Busignies • Vincent Mazel • Bernard Leclerc • Pierre Evesque • Pierre Tchoreloff

Received: 16 April 2010 / Accepted: 23 July 2010 / Published online: 10 August 2010

ABSTRACT

Purpose The pore space anisotropy of pharmaceutical compacts was evaluated in relation to the mechanical property anisotropy.

Methods The topology and the pore space anisotropy were characterized by PGSTE-NMR measurements. Parallelepipedical compacts of anhydrous calcium phosphate (aCP) and microcrystalline cellulose (MCC) were tested on top, bottom and side faces. A microindentation and three-point single beam tests were used to measure Brinell hardness, tensile strength and Young's modulus. All the data were submitted to a statistical analysis to test for significance.

Results The porous structure of MCC compacts was anisotropic, contrary to those of aCP. The analysis of the pore space by PGSTE-NMR method showed that its structural anisotropy was controlled by the behaviour under compaction of the excipients. At the same time, the Young's modulus and the tensile strength were the same whatever the direction of testing. For the aCP compacts, all the faces had the same Brinell hardness. With MCC compacts, only the bottom face showed a lower Brinell hardness.

Conclusions Except for Brinell hardness measured on MCC compacts, the tested samples were characterized by anisotropic mechanical properties when its porous structures were sometimes anisotropic. Then, there is not a straight link between porosity anisotropy and mechanical properties.

KEY WORDS anisotropy · compaction · mechanical property anisotropy · porous structure · pulsed-gradient stimulated-echo NMR

INTRODUCTION

Pharmaceutical compacts are generally obtained by uni-axial compaction of a powder into a die. It is well described that such a process gives compacts with a heterogeneous internal tablet structure. The first density distribution measurement was performed by Train in 1957 (1). Later, modern techniques like NMR microscopy (2,3) and X-ray tomography (4–6) have been applied to pharmaceutical compacts. Nevertheless, the spatial resolution of these techniques is generally too low to make possible the study of the pore space.

Recent works displayed a non-uniform distribution of density and porosity within the compacts in relation to die-wall frictions, particle orientation upon consolidation, distribution of compaction force, shape of die and tooling and conditions of die fill (4–9). At the same time, mechanical properties are known to be dependent on porosity (10). In some works, tablets are shown to have anisotropic mechanical properties (11–17), meaning that the mechanical properties vary with the orientation in which the properties are measured.

P. Porion
Centre de Recherche sur la Matière Divisée—UMR 6619
CNRS and Université d'Orléans
1 bis rue de la Férollerie, 45071 Orléans Cedex 2, France

V. Busignies (✉) • V. Mazel • B. Leclerc • P. Tchoreloff
EA401, Matériaux et Santé, Univ Paris-Sud, Faculté de Pharmacie
5 rue Jean-Baptiste Clément, 92296 Châtenay-Malabry Cedex, France
e-mail: virginie.busignies@u-psud.fr

P. Evesque
Laboratoire de Mécanique: Sols—Structure—Matériaux—UMR 8579, Ecole Centrale de Paris
Grande Voie des Vignes, 92295 Châtenay-Malabry Cedex, France

This variability of mechanical properties is supposed to explain some manufacturing problems observed during compaction processes such as capping and lamination. Due to the impact on the quality of pharmaceutical tablets, the study of a potential anisotropy in the mechanical properties is of interest. Various techniques, mainly compression and indentation testing (14–16,18), have been proposed with this aim in view. Recently, Akseli *et al.* (17) proposed the use of a contact ultrasonic method. Except this last work, it is often difficult to conclude on mechanical property anisotropy due to complicated sample preparations (13), complex experimental setups (11,13), conditions of testing which are not comparable (11) and difficulties of analysing the results (8). Moreover, most studies reported different test methods in the axial and radial directions (11–13). These different testing techniques could interfere with the effect of the testing direction and could induce resulting anisotropy.

In this work, to access the topological information (connectivity and topology) of the porous structure of compacts, we used the pulsed-gradient stimulated-echo (PGSTE) NMR experimental technique. This PGSTE-NMR method is widely applied to various porous media or complex fluids (19–23). At the same time, Young's modulus, tensile strength and Brinell hardness were measured by applying a load on the top, bottom and side faces of parallelepipedical compacts, *i.e.* on the faces parallel or perpendicular to the direction of compaction. Two excipients with different compaction behaviour (anhydrous calcium phosphate and microcrystalline cellulose) were studied to evaluate the impact on the mechanical property anisotropy. The use of a same test method (a three-point single beam test or a microindentation test) in all the tested directions made possible the direct comparison of the mechanical properties in the different directions. The aim of these measurements was to observe if the anisotropy of the porous structure and the mechanical property anisotropy were directly linked.

MATERIALS AND METHODS

Materials

Sieved fractions (100–120 μm) of two common pharmaceutical excipient powders were used: anhydrous calcium phosphate (aCP) (A TAB®, GW930187, Rhodia, France) and microcrystalline cellulose (MCC) (Vivapur 12®, 5601210932, JRS, Germany). Before use, the fractions were stored in a closed chamber with a saturated $NaHSO_4$, H_2O solution corresponding to a relative humidity of about 50% and kept at room temperature (around 20°C) for at least 3 days. The apparent particle density of each fraction was determined using a helium pycnometer (Acupyc 1330, Micromeritics, USA): 2.8103 ± 0.0002 g.cm^{-3} for aCP and 1.5402 ± 0.0005 g.cm^{-3} for MCC.

Compact Preparation

Parallelepipedical tablets were prepared by uni-axial compaction using a hydraulic press (Perrier Labotest, France). The compact size was adapted to the NMR tube (inner diameter of 8.5 mm). In consequence, the punch dimension was 40×5 mm^2, and the mass of powder was adjusted to reach a theoretical thickness of 3 mm for a compact with zero porosity. These dimensions are close to those prescribed in the standard ASTM C1161 (24) to be sure to respect the bending theory.

Prior to compaction, the punch and die surfaces were lubricated with magnesium stearate (NF-BP-MF2 039445, Akcros Chemicals v.o.f., Netherlands). The excipients were compacted under pressures (σ_c) ranging from 25 to 200 MPa. The compact faces were marked *a* (top), *b* (side), *c* (bottom) and *d* (side) to enable testing of compacts in different directions, *(Ox)*, *(Oy)* and *(Oz)* (Fig. 1). Face *a* was perpendicular to the compaction axis *(Oz)* and was in contact with the moving upper punch. After compaction, the compacts were stored for at least 3 days in a closed chamber at a relative humidity of about 50% and at room temperature (around 20°C).

PGSTE-NMR Measurements

In this study, the porous structure of the compacts was characterized by PGSTE-NMR measurements. The porous network of the compacts was indirectly analyzed by the observation of the modification of the diffusion process of molecules in the pore space of the samples. For the compacts, it consists in studying the self-diffusion process of molecules of a NMR-sensitive fluid when this one is confined in the compact porous network. These measurements and their behaviours make possible to obtain pertinent topological information on the porous structure (connectivity, tortuosity) when such results are compared to those observed when the molecules are not confined in the porous network of the material. This last situation corresponds to an isotropic diffusion process in bulk fluid that is characterized by the bulk self-diffusion coefficient of the fluid (noted D_0). On the contrary, for fluid confined in porous media, diffusion is restricted by the solid surfaces bounding the pore space, and this induces a decrease of the apparent self-diffusion as compared to the bulk condition. This fluid must satisfy several properties: it must be NMR sensitive (^{1}H NMR), and it does not modify the porous structure by chemical reaction, dissolution or swelling. The right fluid was chosen during preliminary tests, and its compatibility with aCP and MCC tablets was verified.

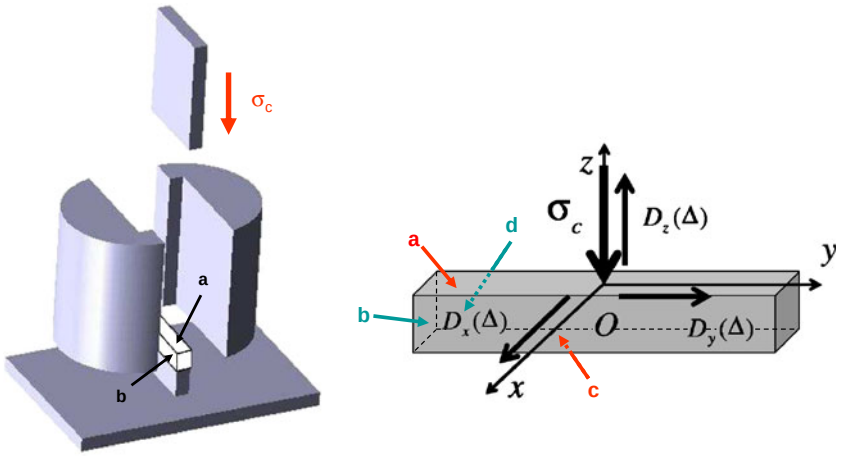

Fig. 1 Schematic of the compact geometry and references axis used for the measurements of the diffusion process in the parallelepipedical tablets and definition of the $D_x(\Delta)$, $D_y(\Delta)$ and $D_z(\Delta)$ self-diffusion coefficients.

For that purpose, before the NMR experiments, the compacts were totally saturated by silicon oil that was introduced in the pore space by a simple impregnation process induced by the capillary effect. It was assumed that the porosity is connected and that all the pore space is impregnated, the closed porosity excepted. The samples were in contact by their flat-bottom face with the silicon oil during 1 week before NMR measurement. After impregnation, the samples were weighed to verify that the porous structure has been filled with oil. It is an important point to consider since the pore accessibility could be limited at high compaction pressure due to percolation (25). For all samples, except those of MCC compacted under 200 MPa, the variation between the calculated porosity and those determined by weighing is equal or lower than 5%. For MCC compacts obtained under 200 MPa, about 75% of the porosity has been filled by the silicon oil. In fact, a pore percolation threshold is not observed for calcium phosphate. Then, all the porosity can be reached. On the contrary, a pore percolation threshold exists for microcrystalline cellulose (25), and the isolated pore clusters cannot be filled by the oil.

The silicon oil (polydimethylsiloxane, Rhodorsil 47V20, Prolabo, France) was characterized by a bulk self-diffusion coefficient (D_0) of 2.73×10^{-11} $m^2.s^{-1}$ at 296 K. After impregnation, the self-diffusion coefficient of the silicon oil molecules was measured by using a PGSTE-NMR pulses sequence (19). In such porous materials, the confined fluids are often characterized by a large difference of values between the two relaxation times T_1 and T_2 and $T_1 \gg T_2$, where T_1 and T_2 are the longitudinal and transverse relaxation times, respectively (19). For example, in these pharmaceutical compacts, the typical relaxation measurements of the silicon oil molecules confined in the pore space gave a ratio $T_1/T_2 \approx 30$ (with $T_1 \approx 1{,}000$ ms and $T_2 \approx$ 35 ms). In that case, it is worth noting that the standard pulsed-gradient spin-echo (PGSE) NMR sequence is not suitable to measure with good accuracy the self-diffusion coefficient at long diffusion time Δ due to the short T_2 value. Then, it shall use a modified PGSE-NMR sequence (26), which generates a stimulated echo (STE) that makes possible to significantly enhance the NMR echo signal. The PGSTE-NMR sequence, with the different times and parameters used in this study, was represented in previous work (see Fig. 2 in Ref. (9)).

The self-diffusion coefficients $D(\Delta)$ were calculated by measuring the decrease in the NMR echo signal intensity through increasing magnetic field gradients. In a chosen direction (O_i), the self-diffusion coefficients were obtained by nonlinear least-square fitting of the echo attenuation $E(q,\Delta)$ as

$$E(q,\Delta) = \frac{I(q,\Delta)}{I(0,\Delta)} = \exp\left[-4\pi^2 q^2 \mathbf{e}_i^T \mathbf{D} \mathbf{e}_i (\Delta - \delta/3)\right] \qquad (1)$$

where $I(q,\Delta)$ and $I(0,\Delta)$ are the echo intensities, respectively, measured with and without the field gradient; $q = \gamma g \delta / 2\pi$,

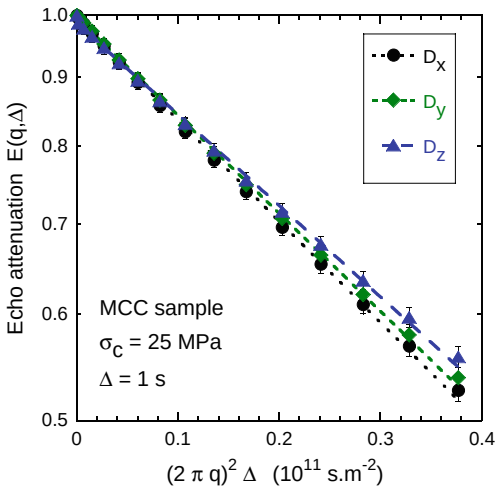

Fig. 2 Examples of echo amplitude attenuation $E(q,\Delta)$ as a function of $4\pi^2q^2\Delta$ with $q = \gamma g\delta/2\pi$ measured for MCC sample at $\sigma = 25$ MPa along the three distinct perpendicular directions (O_x), (O_y) and (O_z) for a diffusion time $\Delta = 1$ s. The self-diffusion coefficients D_x, D_y and D_z are calculated by least-squares fitting (*straight lines*).

here g is the intensity of the pulsed magnetic field gradient, δ its duration, γ the gyromagnetic ratio of the proton ($\gamma = 2.6752 \times 10^8$ rad.s^{-1}.T^{-1}), $\mathbf{e}_i$ the unitary vector along the chosen direction (O_i), $\mathbf{e}_i^T$ its transposed vector, $\mathbf{D}$ is the self-diffusion tensor and Δ is the diffusion time. In this sequence, the higher value of Δ is experimentally limited by the T_1 value.

In this work, the upper value of the diffusion time Δ was taken at 5,000 ms that corresponded to five times the longitudinal relaxation time T_1 ($T_1 \approx 1{,}000$ ms). All measurements were performed on a Bruker DSX 100 spectrometer operating at 100 MHz for the proton, and a 10 mm microimaging probehead (Micro5 Bruker) with gradient coils in the three perpendicular directions was used to generate magnetic field gradient in any arbitrary direction (O_i). The temperature was fixed at 296 K. For a given direction (O_i), the self-diffusion coefficient D was extracted from a series of measurements involving different g values (16 steps) with the duration δ fixed at 5 ms. As we already explained, the self-diffusion coefficient was extracted from experimental data by a simple linear fit of $\ln(E(q,\Delta))$ as a function of $4\pi^2 q^2 \Delta$ (see Fig. 2 for example). More details about the experimental procedure can be found in ref. (9). Due to the symmetry of the parallelepipedical samples (Fig. 1), for each diffusion time Δ, the self-diffusion coefficients were measured along three distinct perpendicular directions: two distinct perpendicular directions (O_x) and (O_y) in the plane (xOy) and along the direction (O_z) corresponding to the compression axis. Only samples obtained under 25 and 200 MPa were selected for PGSTE-NMR experiments.

Mechanical Property Measurements

Mechanical properties were studied after total elastic recovery of the compacts. The experimental procedure and the evaluation of the mechanical properties were described in detail in previous works (27,28). A micropress was employed to measure the mechanical properties. The instrumentation makes possible to draw the force-displacement curves. The applied forces are in the range of 0–500 N. The resolution of the force transducer is 0.01 N, and its nominal sensitivity is 2 mV. V^{-1}. The accuracy of the displacement transducer is ±1 μm. Three mechanical properties were measured by a unified method in axial and radial directions. Then, a direct comparison was possible between the mechanical properties measured in different directions. These mechanical properties were obtained by applying a load on the top (face *a*), bottom (face *c*) and side faces (faces *b* and *d*) of the compacts to evaluate the mechanical property anisotropy. The Young's modulus (E) and the tensile strength (σ_r) were obtained using a three-point single-beam test. The compacts were placed and centred on the three-point system and stressed using a 2 mm flat punch at a constant velocity of 0.050 mm. min^{-1}. To obtain only the elastic response of the compact, a series of loading/unloading cycles was applied, 5 cycles for MCC compacts and 3 cycles for aCP compacts. The Young's modulus was obtained from the slope of the loading part of the last loading/unloading cycle:

$$E = \frac{F.p^3}{4.\delta.h^3.l} \tag{2}$$

F is the maximum applied load, corresponding to 80% of the load that causes compact fracture (F_r); p is the distance between the two supports (34.12 mm); δ is the central deflexion; and h and l are the thickness and the width of the sample when the tested face is facing the direction of loading.

The tensile strength was obtained from the force that caused compact fracture (F_r):

$$\sigma_r = \frac{3.F_r.p}{2.l.h^2} \tag{3}$$

Except F_r, the other parameters are those of Eq. 2.

The Brinell hardness (H_b in MPa) was obtained using a microindentation test. A stress was applied on the centre of the tested face by a spherical indenter with a 2.38 mm diameter (D) at a rate of 0.06 mm. min^{-1}. The maximal displacement of the indenter and the relaxation time were adjusted to the excipient (27). For MCC compacts, the indenter displacement was 0.1 mm, and the relaxation time was 5 min. For aCP compacts, the indenter displacement was 0.06 mm, and the relaxation time was 1 min. The Brinell hardness was calculated from the maximal applied load (F) and the diameter of the indentation surface (d):

$$H_b = \frac{2.F}{(\pi.D).(D - \sqrt{D^2 - d^2})} \tag{4}$$

For each mechanical property, each pressure target and each compact face, three tablets were tested. Then, the mechanical properties were plotted *versus* the compaction pressure. The degree of anisotropy for each mechanical property at a given compaction pressure was quantified by the following parameter, α:

$$\alpha = \frac{X_a}{X_i} \tag{5}$$

with X_a, the mean of the mechanical property (Young's modulus, tensile strength or Brinell hardness) obtained by applying the load on face *a* at a given compaction pressure, and X_i, the mean of the same mechanical property obtained by applying the load on face *b*, *c* or *d* at the same compaction pressure.

The ratio α is unity for homogeneous compacts. The compact is considered to have anisotropic mechanical properties when α value differs from unity.

Statistical Analysis

Data were subjected to statistical analysis using Microsoft Office Excel 2003 (Microsoft Corporation, US) and OriginPro 8 (OriginLab Corporation, US) softwares.

ANOVA one-way analysis (analysis of variance) was used to test for significance (29). In this analysis, the statistical null hypothesis was that the means of the measured mechanical property were the same for the data obtained on two different faces (*i.e.* for the two groups of data). The alternative hypothesis was that they were not the same. The mean of the data within each group was calculated, and the variance among these two means was compared to the average variance within the two groups. The corresponding statistic parameter was the ratio of the variance among means divided by the average variance within the two groups (F-ratio). The probability of obtaining the observed F-ratio under the null hypothesis was calculated (probability level, p). By setting a limit on the probability level (typically 0.01 or 0.05), a critical F-ratio was determined with standard tables. Values of F-ratio greater than the critical value mean the rejection of the null hypothesis. It corresponds to small values of p (*i.e.* $p<0.01$ or 0.05). This implies that the means differ by more than would be expected by chance alone and are significantly different.

The assumptions of the ANOVA one-way analysis (normality and homoscedasticity) were first controlled by a Shapiro-Wilk test for normality and a Fisher-Snedecor test for homoscedasticity. When the normality was not verified, a non-parametric Kruskal-Wallis test was used to compare the data of the two groups. It corresponds to a one-way analysis of variance with the data replaced by their ranks. The corresponding ratio and probability (Q-ratio and p) were calculated.

RESULTS AND DISCUSSION

Characterization of the Pore Space by PGSTE-NMR Measurements

As previously mentioned, due to the symmetry of the parallelepipedical samples, the self-diffusion coefficients D_i with $i\in\{x,y,z\}$ were measured along three distinct perpendicular directions related to the uni-axial compaction process (Fig. 1), and they were evaluated for a diffusion time Δ varying from 30 ms to 5,000 ms. The evolutions of the self-diffusion coefficients in the directions perpendicular ($D_x(\Delta)$ and $D_y(\Delta)$) and parallel ($D_z(\Delta)$) to the compaction axis (O_z) as a function of the diffusion time are reported in Fig. 3. Concerning the measurements in the *xOy* plane, $D_x(\Delta)$ appeared to be equal to $D_y(\Delta)$ within the experimental error, indicating that the porous structure (connectivity and topology) of the tablets looked isotropic in the *xOy* plane, *i.e.* perpendicular to the compaction axis (O_z). To simplify the discussion, the mean self-diffusion in the *xOy* plane, noted $D_\rho(\Delta)$, was defined as $D_\rho(\Delta) = \big(D_x(\Delta) + D_y(\Delta)\big)/2$, and in the following, only the evolutions of $D_\rho(\Delta)$ and $D_z(\Delta)$ will be analyzed and discussed in this paper.

First, for all the samples, when the diffusion time was increased from 30 ms to 5,000 ms, the self-diffusion coefficients $D_i(\Delta)$, with $i\in\{\rho,z\}$ decreased continuously to reach an asymptotic value (when Δ was greater than 2,000 ms). This dependence of $D_i(\Delta)$ on the diffusion time is the fingerprint of the restricted diffusion phenomena in space characterized by large scale homogeneity (19). Such behaviour is often observed in porous materials (30). Indeed, at very short time Δ, the molecules of the fluid do not have enough time to entirely explore the pore space, and the diffusion process is little perturbed by the inner wall of the pores. $D_i(\Delta)$ was then equal to D_0, when Δ was small $\Delta\rightarrow 0$, i.e. the value for non-confined silicon oil (bulk condition). Consequently, it is expected that the bulk self-diffusion coefficient D_0 will be reached at $\Delta\rightarrow 0$, in the limit when the molecules of liquid do not undergo physisorption or chemisorption at the solid surface of the solid surface of pores and in the limit of a large volume-to-surface ratio. At this stage, we would like to make two comments on the influence of the physisorption and the chemisorption phenomena on the self-diffusion measurements by PGSTE-NMR method to probe a porous structure. First, the physisorption is a reversible process that can be characterized by a residence time on the surface. For physisorption phenomena, the typical residence time value can be estimated to the microsecond about for its upper limit. Compared to the time scale of the NMR experiments (30–5,000 ms about for the diffusion time Δ), this typical residence time is very small (few orders of magnitude), so that the physisorption phenomena does not interfere with the self-diffusion measurement by PGSTE-NMR method. Second, the possible chemically adsorbed PDMS molecules do not move (no translation motion), and they do not contribute to the signal of the NMR PGSTE method for the self-diffusion measurements that is only sensitive of translation motion of the chemical species.

However, owing to the technical limitations of the PGSTE-NMR experiments, which impose a diffusion time Δ greater than few milliseconds (here $\Delta\geq 30$ ms), it was impossible to reach this regime at very small times. At larger time Δ, the free molecules begin to encounter the walls, and their pathway is restricted. In this intermediate regime, the diffusion is then limited by the restriction of

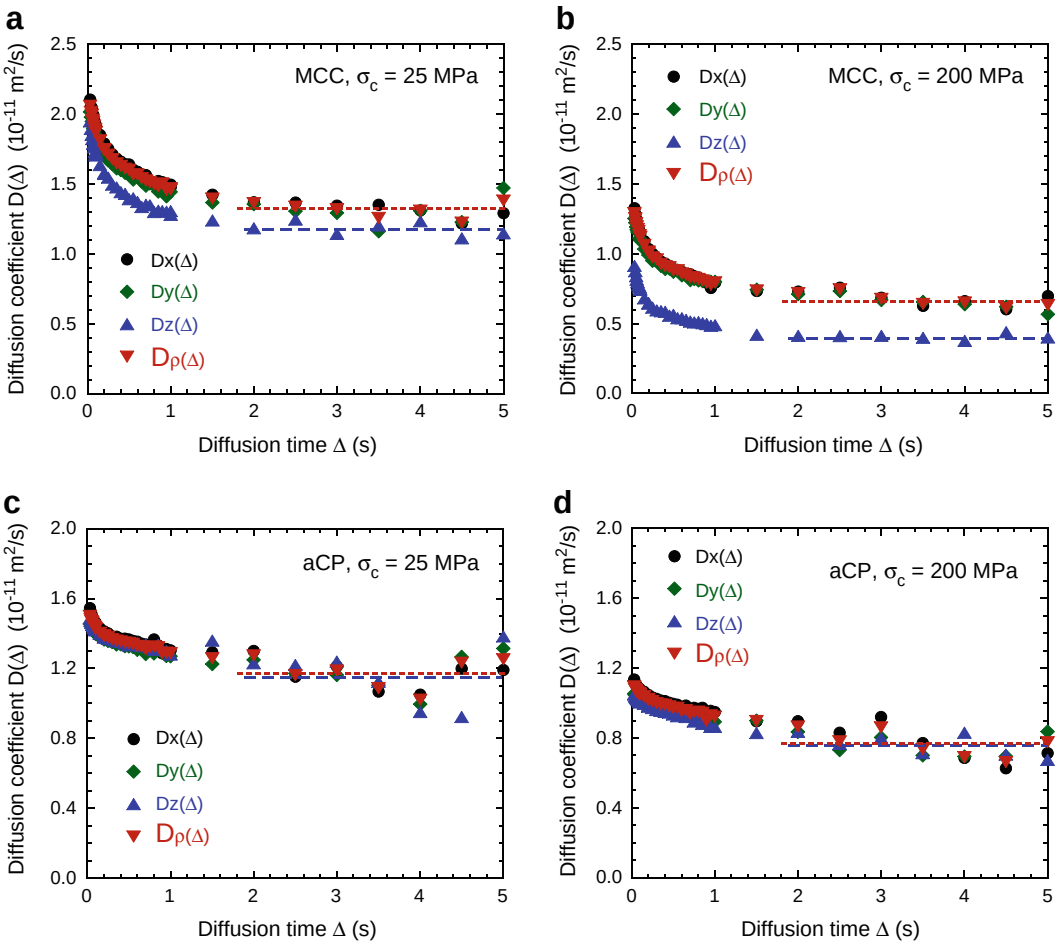

Fig. 3 Evolution of the self-diffusion coefficients $D_i(\Delta)$ with diffusion time (Δ) for the compacts of MCC (**a**: $\sigma_c = 25$ MPa and **b**: $\sigma_c = 200$ MPa) and aCP (**c**: $\sigma_c = 25$ MPa and **d**: $\sigma_c = 200$ MPa). The asymptotic values of the self-diffusion coefficients D_i^∞ are evaluated as the mean value of $D_i(\Delta)$ for a time diffusion Δ varying between 2 and 5 s (see the dashed lines, in blue D_z^∞ for the direction parallel to the compaction axis and in red D_ρ^∞ for the direction perpendicular to the compaction axis).

motion and by the distribution of initial positions that both modify the statistic of collisions on the walls during the time Δ at which the NMR measurement is performed. This phenomenon reduces the value of the self-diffusion coefficients: $D_i(\Delta)$ is always smaller than D_0. $D_i(\Delta)$ decreases when the diffusion time Δ increases until the diffusion time is sufficiently large so that the molecules explored the whole representative elementary volume (REV) of the sample for the diffusion process. As the fluid molecules can only invade the open pore structure, the diffusion at large time-scale Δ shall reflect this fact, and the effect of the pore space structure can be averaged, so that $D_i(\Delta)$ does not depend on the time Δ anymore; this is an asymptotic behaviour.

In the studied samples, this regime occurred for Δ greater than 2,000 ms. The self-diffusion coefficient then reached its asymptotic value along the axis (O_i) noted D_i^∞ with $i \in \{\rho,z\}$. These asymptotic values D_i^∞ were evaluated for the two excipients MCC and aCP as the mean value of $D_i(\Delta)$ for the diffusion time varying between 2 s and 5 s, assuming that the cross-over between the two last regimes appeared for a critical value of the diffusion time Δ_c equal to 2 s (see the asymptotic behaviours in Fig. 3). It was then possible to calculate a characteristic diffusion length $\ell_i = \sqrt{2D_i^\infty \Delta_c}$ which corresponds to the minimum length for which the asymptotic regime was reached. From this set of characteristic lengths, the size of the representative elementary volume (REV) above which the sample could be seen as homogeneous material for the diffusion transport properties was defined. Taking into account the symmetry of the samples, this REV could be defined as $V_{REV} = \ell_\rho^2 \ell_z$. The results were summarized in Table I. For the two excipients, one observed a reduction of the REV value when the compaction pressure was increased from 25 MPa to 200 MPa, these variations of volume were more important for MCC samples ($\Delta V_{REV} = -70\%$) than for aCP samples ($\Delta V_{REV} = -47\%$). In other words, at high compaction pressure, the sample can be seen as homogeneous material at smaller scale. It was also interesting to compare the values

Table I Asymptotic Values D_z^∞ and D_ρ^∞ of the Self-Diffusion Coefficients in Different Directions (Parallel to (O_z) or Perpendicular to it (O_ρ), i.e. in the xOy Plane) Corresponding to the Behaviour for the Long Diffusion Time Δ, Characteristic Diffusion Lengths ℓ_z and ℓ_ρ, and Evaluations of the Representative Elementary Volume Size V_{REV} (see text) at Two Compaction Pressures (25 MPa, 200 MPa) of the Two Excipients Studied (aCP and MCC)

Compaction pressure (MPa)	D_ρ^∞ (10^{-11}m^2/s)	ℓ_ρ (μm)	D_z^∞ (10^{-11}m^2/s)	ℓ_z (μm)	$V_{REV} = \ell_\rho^2 \ell_z$ (μm^3)
Anhydrous calcium phosphate (aCP)					
25 MPa	1.174	6.85	1.153	6.79	318.91
200 MPa	0.767	5.54	0.761	5.52	169.33
Microcrystalline cellulose (MCC)					
25 MPa	1.314	7.25	1.182	6.88	361.33
200 MPa	0.669	5.17	0.407	4.04	107.92

of D_i^∞ according to the compaction pressures. For the MCC and aCP samples, these D_i^∞ values decreased as expected when the compaction pressure increased from 25 MPa to 200 MPa (Fig. 3). This behaviour means that the porosity reduces and the connectivity becomes lower when the tablet was compacted with a higher pressure. Concerning the difference of D_i^∞ values according to the direction of the measurement, D_ρ^∞ was always higher than D_z^∞ for MCC samples, and the difference $D_\rho^\infty - D_z^\infty$ increased with the compaction pressure. On the contrary, for aCP samples, the D_i^∞ values were the same in any case. To quantify the structural anisotropy of the pore space, the diffusion anisotropy factor λ was introduced as the ratio:

$$\lambda = D_{\max}^\infty / D_{\min}^\infty = D_\rho^\infty / D_z^\infty \tag{6}$$

where $D_{\min}^\infty$ and $D_{\max}^\infty$ are, respectively, the maximal and the minimal value of the macroscopic self-diffusion measured in the two principal directions. When the pore space is isotropic, $D_{\min}^\infty = D_{\max}^\infty = D^\infty$ and $\lambda = 1$. This diffusion anisotropy factor λ is expected to increase with the anisotropy of the pore space. The variations of λ with the compaction pressure were shown in Table II. For MCC samples, λ was greater than 1, and it increased from 1.11 to 1.64 when the compaction pressure was ranged from 25 MPa to 200 MPa. For aCP samples, λ was almost equal to 1 for all compaction pressures. This difference observed between the two excipients could be explained by their mechanical properties which induced a change of the nature of particle deformation under compression. Indeed, as already mentioned, MCC is a plastic material, whereas aCP is a brittle excipient.

Another way to describe the porous structure is through the tortuosity concept that was originally proposed by Carman in 1937 (31). The tortuosity characterizes the mean trajectory length of the fluid in porous material; it is noted θ. With this definition, the real length L^*, covered by a fluid to go through pores space between two parallel planes perpendicular to the mean flow, is θ times greater than the straight Euclidian length L separating these planes; $\theta = L^*/L$ is a dimensionless number. The tortuosity is equal to unity when the porous structure is made of parallel linear tubes, but this parameter increases when the porous structure becomes different of linear porosity (Fig. 4). This definition can be extended to take into account the anisotropy of the porous structure. Using the PGSTE-NMR measurements, this tortuosity parameter can be used as a way to quantify the global diffusion process in the following manner. Indeed, from D_0 and the self-diffusion coefficient calculated at long observation time, D_i^∞ can be used to estimate directly another parameter, the tortuosity

Table II Asymptotic Values D_ρ^∞ and D_z^∞ of the Self-Diffusion Coefficients Corresponding to the Behaviour for the Long Diffusion Time Δ, Tortuosity Factors τ_ρ and τ_z, Tortuosities θ_ρ and θ_z, Diffusion Anisotropy Factor λ and Relative Difference of the Tortuosity Factors $\Delta\tau$ (see text) at Two Compaction Pressures (25 MPa, 200 MPa) of the Two Excipients Studied (aCP and MCC). The Measured D_0 Value is 2.73×10^{-11} m^2/s

Compaction pressure (MPa)	D_ρ^∞ (10^{-11}m^2/s)	τ_ρ	θ_ρ	D_z^∞ (10^{-11}m^2/s)	τ_z	θ_z	λ	$\Delta\tau$ (%)
Anhydrous calcium phosphate (aCP)								
25 MPa	1.174	2.33	1.52	1.153	2.37	1.54	1.02	1.79
200 MPa	0.767	3.56	1.89	0.761	3.59	1.89	1.01	0.87
Microcrystalline cellulose (MCC)								
25 MPa	1.314	2.08	1.44	1.182	2.31	1.52	1.11	10.03
200 MPa	0.669	4.08	2.02	0.407	6.71	2.59	1.64	39.12

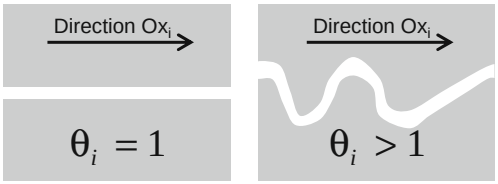

Fig. 4 In porous material, the tortuosity θ characterizes the trajectory of a fluid (or the molecules for a gaseous phase) inside the pore space. More θ is large, more the trajectory deviates from the straight line to cross the sample.

factor (32–34) defined as $\tau_i = D_0/D_i^{\infty}$ in the direction (O_i). The tortuosity θ_i and the tortuosity factor τ_i of the pore space are then related to the self-diffusion coefficients by the following equation:

$$\theta_i^2 = \tau_i = D_0/D_i^{\infty} \quad (7)$$

where D_0 is the self-diffusion of the fluid in the bulk situation (*i.e.* when it is not confined to the pore space, $D_0 = 2.73 \times 10^{-11}$ $m^2.s^{-1}$) (9). Table II reported the experimental finding for each sample in the different directions at two different compression pressures. For all samples, τ_z was always higher than τ_ρ. Moreover, the relative difference, defined as $\Delta\tau = (\tau_z - \tau_\rho)/\tau_z$ (Table II), increased with the compaction pressure, and it was also larger for MCC excipient (for MCC: $\Delta\tau$=10% at 25 MPa and $\Delta\tau$=39% at 200 MPa). Indeed, for the aCP samples, the difference $\Delta\tau$ was lower than 2% (for aCP: $\Delta\tau$=1.8% at 25 MPa and $\Delta\tau$=0.9% at 200 MPa). These results also confirmed that the pore space for the brittle excipient (*i.e.* aCP) was homogeneous and isotropic, since no variations were observed along the two principal directions of measurement.

In conclusion, the diffusion in the pore space depended on the compaction behaviour of the compacted materials. With MCC excipient, which is a plastic material, the anisotropy of the self-diffusion coefficients was observed. Then, it could be concluded that the pore space of MCC parallelepipedical compacts was anisotropic. A similar conclusion was obtained by Djemai and Sinka (3) with a grade of microcrystalline cellulose. They concluded that the density distributions inside compacts were complex and resulted from various factor like die-wall frictions and tablet shape. On the contrary, the diffusion results showed that the pore space of aCP compacts was isotropic. The anisotropy probably resulted from the plastic behaviour of MCC under pressure. A brittle material like aCP excipient led to isotropic pore space. Moreover, the same trend was previously observed on cylindrical compacts composed of the same excipients (9). Then, the pore space seemed to be more affected by the material deformation behaviour than by the tablet geometry. In regard to previous published works (11–17), anisotropy of the pore space was expected to have an effect on some tablet's properties. Then, discussion in the next part is interested in the connection with anisotropy of the pore space and a potential anisotropy of the mechanical properties.

Mechanical Property Anisotropy

As already mentioned in the Introduction, mechanical property anisotropy could be expected due to compaction process, die-wall frictions, compact geometry and different compaction behaviours of the excipients under pressure (3–11,17). In addition, compaction behaviour can induce anisotropy of the pore space (case of MCC compacts).

In this study, a simple method was proposed to test the sample in four measurement directions. The same test was used in axial and radial directions. Then, a direct comparison was possible between the measured mechanical properties, and differences on mechanical properties in axial direction (Oz) and radial directions (Ox) were not induced by the test. Due to the symmetry of the compacts, identical results for tests performed on faces *b* and *d* were expected. This result was proved by the statistical analysis performed on the experimental results (data not shown).

Tensile strength, Young's modulus and Brinell hardness of aCP and MCC compacts for the four directions of loading were evaluated, and the results are shown in Figs. 5, 6 and 7. Corresponding F-ratio and *p* value are listed in Tables III, IV and V.

Tensile Strength

The samples of MCC and aCP presented no effect of the tested direction on the tensile strength values (Fig. 5). In the axial direction, the tensile strength values were in accordance with previous results obtained with larger samples (28,35). On the whole, the statistical analysis gave p values higher than 0.01 (and often higher than 0.1). It confirmed that the axial and radial tensile strengths were equal at a given compaction pressure. Then, for this property, all the compacts (aCP and MCC) had isotropic tensile strength, and α values were almost equal to unity. It is not surprising, since the fracture begins from the large defect in the compact (36); hence, it may appear anywhere independently of the direction, even if the compressed compacts have some non-uniform density distribution (6,37). Therefore the tensile strength values are not direction dependent. In other words, the tensile strength is a mechanical property which characterizes the mean volume of the compact and which does not depend on the mean local pore space, but rather on some large (but rare) defect in the pore space structure.

In contrast, other works generally reported that tensile strength tests revealed mechanical property anisotropy in the compacts (11–14). A first variation can be due to the

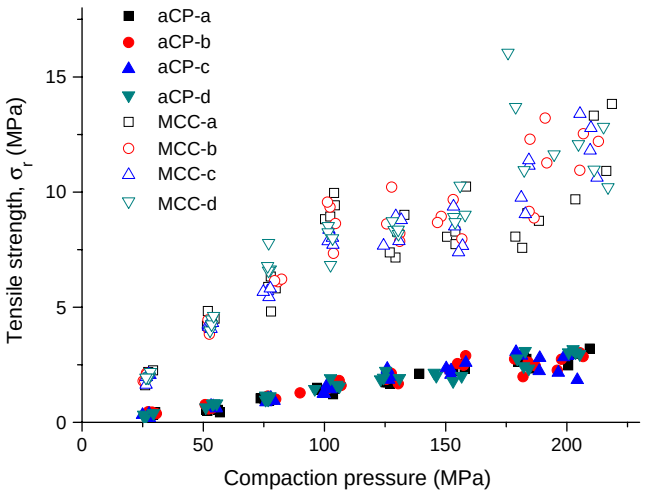

Fig. 5 Evolution of tensile strength with the applied compaction pressure for the compacts of MCC and aCP depending on the testing direction (on face a, b, c or d).

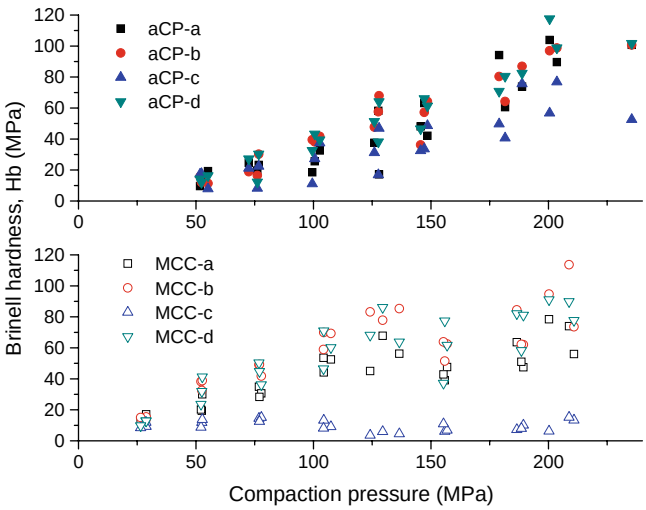

Fig. 7 Evolution of Brinell hardness with the applied compaction pressure for the compacts of MCC and aCP depending on the testing direction (on face a, b, c or d).

tablet geometry and size. It was previously observed that different strengths were obtained with a three-point single-beam test and a diametral compression test (35,38). In some cases, the differences with our observations (obtained with a unified test method) were likely due to the use of different test methods in the axial and radial directions (11–13). These different experimental approaches and testing techniques could interfere with the effect of the testing direction. It should even be supposed that the anisotropy was more induced by the testing method than by the direction of testing. The strength measured by compression was an example (8,14). By compression, the force at which fracture occurred was registered, but it was not possible to easily calculate the corresponding strength, since the fracture surfaces were many and complex (contrary to those observed when a cylindrical compact was subjected to a diametral compression test (39)). Generally, the corresponding stress was derived from the crushing force divided by the original cross-sectional area of the sample. This is a questionable way of calculation, since it defines the means of the crushing strength so that any difference in different direction does not sign exactly the mechanical property anisotropy of samples. Moreover, as noted by Galen and Zavaliangos (13), the extent of the strength anisotropy depends on the compaction path, which is another point which could justify the variability between different studies.

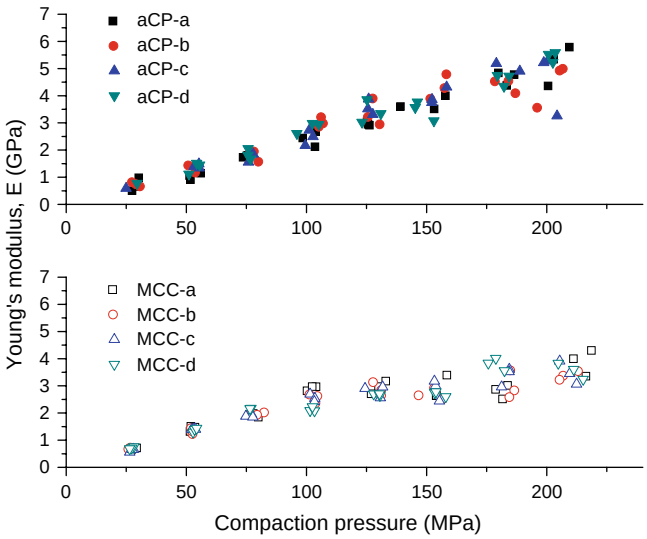

Fig. 6 Evolution of Young's modulus with the applied compaction pressure for the compacts of MCC and aCP depending on the testing direction (on face a, b, c or d).

Young's Modulus

For MCC compacts, the values in the axial direction were the same as those previously observed with larger samples. The Young's modulus of aCP compacts was slightly higher than the values obtained with larger sample (28,35). Once again, in the case of Young's modulus measurements (Fig. 6), no variation with orientation was observed for the compacts of aCP and MCC (p values generally higher than 0.01). The mean α values of 0.9 (aCP) and 1.0 (MCC) induced that aCP and MCC compacts had Young's modulus isotropy. Then, compacts with an anisotropic pore space (for example, MCC compacts) were not characterized by anisotropy of the elasticity.

The Young's modulus anisotropy on pharmaceutical compacts is little studied. We can cite the work of Akseli *et al.* (17) in which the sample anisotropy was characterized through the measurement of the velocity of an ultrasound pulse propagating the tested compact in different directions.

Table III ANOVA (F-Ratio and Probability Level) Results and Anisotropy Parameter: Effect of the Tested Direction on the Young's Modulus in the Case of Compacts of the Two Excipients

Compaction pressure (MPa)	(a) × (b)			(a) × (c)			(a) × (d)		
	F- ratio	Probability level (p)	Anisotropy parameter (α)	F- ratio	Probability level (p)	Anisotropy parameter (α)	F- ratio	Probability level (p)	Anisotropy parameter (α)
Anhydrous calcium phosphate (aCP)									
25	0.04	0.853	1.0	0.19	0.708	1.2	0.05	0.845	0.9
50	7.40	0.053	0.8	20.74	0.010	0.7	5.21	0.084	0.8
75	0.09	0.773	1.0	0.04	0.858	1.0	0.36	0.580	1.0
100	10.09	0.034	0.8	0.05	0.825	1.0	4.71	0.096	0.8
125	1.80	0.251	0.9	12.32	0.025	0.8	3.19	0.148	0.9
150	4.19	0.110	0.9	1.42	0.300	0.9	0.85	0.408	1.1
175	1.81	0.249	1.1	3.24	0.170	0.9	0.09	0.774	1.0
200	1.14	0.346	1.1	0.54	0.504	1.1	0.42	0.552	0.9
Microcrystalline cellulose (MCC)									
25	0.88	0.402	1.0	1.37	0.307	1.1	1.99	0.231	0.9
50	1.51	0.286	1.1	0.22	0.662	1.0	0.62	0.473	1.0
75	0.54	0.503	1.0	0.38	0.569	1.0	3.00[a]	0.317[a]	0.9
100	10.84	0.030	1.1	14.84	0.018	1.1	124.45	<0.001	1.4
125	0.16	0.708	1.0	0.63	0.472	1.1	3.84	0.121	1.1
150	0.52	0.509	1.1	<0.01	0.957	1.0	0.51	0.515	1.1
175	0.34	0.591	0.9	5.04	0.088	0.8	25.24	0.007	0.7
200	2.98	0.159	1.2	1.20	0.335	1.1	0.99	0.376	1.1

[a] Values (Q-ratio and probability level) obtained with a Kruskal-Wallis test when the normality was not verified

Table IV ANOVA (F-Ratio and Probability Level) Results and Anisotropy Parameter: Effect of the Tested Direction on the Tensile Strength in the Case of Compacts of the Two Excipients

Compaction pressure (MPa)	(a) × (b)			(a) × (c)			(a) × (d)		
	F- ratio	Probability level (p)	Anisotropy parameter (α)	F- ratio	Probability level (p)	Anisotropy parameter (α)	F- ratio	Probability level (p)	Anisotropy parameter (α)
Anhydrous calcium phosphate (aCP)									
25	3.59	0.107	0.8	0.42	0.544	1.1	0.23	0.652	1.1
50	9.51	0.021	0.8	21.07	0.004	0.8	29.36	0.002	0.7
75	3.38	0.116	0.9	0.09	0.774	1.0	1.91	0.216	0.9
100	5.96	0.050	0.8	<0.01	0.948	1.0	4.15	0.088	0.9
125	4.28	0.084	0.9	11.86	0.014	0.8	10.07	0.019	0.9
150	2.38	0.173	0.9	0.02	0.891	1.0	6.92	0.039	1.2
175	0.79	0.409	1.1	0.38	0.559	1.0	0.04	0.856	1.0
200	0.59	0.470	1.1	2.36	0.175	1.2	1.00	0.356	0.9
Microcrystalline cellulose (MCC)									
25	0.11	0.749	1.0	0.13	0.728	1.0	<0.01	0.951	1.0
50	3.79	0.099	1.1	4.02	0.092	1.1	0.67	0.445	1.0
75	1.38	0.293	0.9	0.03	0.873	1.0	8.45	0.027	0.8
100	1.02	0.351	1.1	19.19	0.005	1.2	9.38	0.022	1.2
125	1.30	0.298	0.9	0.47	0.519	1.0	1.04	0.348	0.9
150	0.12	0.739	1.0	0.23	0.647	1.0	0.93	0.373	0.9
175	5.19	0.063	0.8	9.10	0.023	0.8	15.53	0.008	0.6
200	0.07	0.803	1.0	0.03	0.857	1.0	0.13	0.729	1.0

Table V ANOVA (F-Ratio and Probability Level) Results and Anisotropy Parameter: Effect of the Tested Direction on the Brinell Hardness in the Case of Compacts of the Two Excipients

Compaction pressure (MPa)	(a) × (b)			(a) × (c)			(a) × (d)		
	F- ratio	Probability level (p)	Anisotropy parameter (α)	F- ratio	Probability level (p)	Anisotropy parameter (α)	F- ratio	Probability level (p)	Anisotropy parameter (α)
Anhydrous calcium phosphate (aCP)									
25	_ [a]	_ [a]	_ [a]	_ [a]	_ [a]	_ [a]	_ [a]	_ [a]	_ [a]
50	0.30	0.612	1.1	0.01	0.920	1.0	0.03	0.870	1.0
75	0.02	0.892	1.0	1.21	0.333	1.3	0.01	0.907	1.0
100	11.57	0.027	0.6	< 0.01	0.978	1.0	6.38	0.065	0.7
125	2.32	0.203	0.7	0.16	0.707	1.2	0.93	0.389	0.7
150	0.02	0.899	1.0	2.48	0.190	1.3	0.63	0.470	0.9
175	< 0.01	0.937	1.0	2.11	0.220	1.4	0.03	0.876	1.0
200	0.02	0.881	1.0	17.33	0.014	1.6	1.20	0.335	0.9
Microcrystalline cellulose (MCC)									
25	0.02	0.893	1.0	7.75	0.050	1.5	2.66	0.178	1.2
50	11.26	0.028	0.6	10.01	0.034	2.0	2.16	0.216	0.7
75	24.12	0.008	0.7	67.70	0.001	2.2	547.83	< 0.001	0.4
100	11.82	0.026	0.8	139.13	< 0.001	4.9	1.40	0.302	0.8
125	13.77	0.021	0.7	60.95	0.001	12.0	2.97	0.160	0.8
150	12.15	0.025	0.7	148.21	< 0.001	5.4	1.69	0.263	0.7
175	3.05	0.185	0.8	83.29	< 0.001	6.4	4.60	0.098	0.7
200	3.32	0.143	0.7	61.30	0.001	6.0	4.28	0.107	0.8

[a] Data not available due to the lack of cohesion of the compacts

For Avicel PH102® (a grade of MCC with irregular particle shape) cubic compacts, the axial velocity was found different than those determined in the radial directions. Anisotropy of the Young's modulus of MCC compacts and a non-uniform density distribution in the compact structure were deduced. Other work on elastic anisotropy of non-pharmaceutical powders undergoing uniaxial compaction (40) suggested that the anisotropy of elastic properties may be influenced by differences in compaction techniques or anisotropic characteristics of the powders like non-isometric particle shape. It was also discussed that a direct relationship between wave speed and Young's modulus assumes a homogeneous and isotropic propagating medium; in consequence, these assumptions limit the application of such relationship for compacted powders (40).

Brinell Hardness

Concerning Brinell hardness (Fig. 7), no difference was seen when the direction of testing was changed for aCP compacts. The corresponding p values were in most cases widely higher than 0.01, and α was about unity. The hardness values were always higher than those proposed by Aulton (41) for compacts obtained under a same compaction pressure (top face tablets obtained under 175 MPa gave Brinell hardness of 50.7 MPa for calcium phosphate and 35.5 MPa for microcrystalline cellulose). In the two cases, Brinell hardness was measured, but it is well known that the result depends on the indentation depth and the indenter size (16). For MCC samples, the indentations on the different faces gave the same values of Brinell hardness except on face *c*. The

Table VI Estimation of the Measurement Direction Impact on the Mechanical Anisotropy

	Young's modulus (E)	Tensile strength (σ_r)	Brinell hardness (Hb)
Anhydrous calcium phosphate (aCP)			
Axial × Axial	–	–	–
Axial × Radial	–	–	–
Microcrystalline cellulose (MCC)			
Axial × Axial	–	–	+
Axial × Radial	–	–	–

Key: (−), no significant impact; (+) significant impact

difference in axial direction was observed when compaction pressures were higher than 75 MPa ($p \leq 0.001$ if 25 and 50 MPa were excluded and mean α value ~ 5). However, the comparison of the axial and radial directions indicated that concerning the Brinell hardness, the MCC compacts were probably more anisotropic than those of aCP ($\alpha_{(a\text{-}b)} \sim 0.8$ for MCC compacts and $\alpha_{(a\text{-}b)} \sim 1.0$ for aCP compacts).

The indentations on the top and side faces of the aCP and MCC compacts showed that these surfaces had the same hardness. Then, the die-wall frictions do not impact the hardness of the side faces, keeping in mind that the lubrication of the die surfaces before compaction might reduce the effect of friction.

With the two excipients, we also noticed a considerable scatter for the hardness results. Due to axial transmission during compaction, a lower hardness on the bottom face was expected. Previous work (35) showed that the axial transmission was slightly higher for MCC than aCP (but near 90%). Then, the axial transmission did not explain the experimental results.

To our knowledge, there are few works about anisotropy of indentation hardness of pharmaceutical compacts. One should cite those of Aulton (41), Mullarney and Hancock (14) and Lee (16). Nevertheless, their conclusions were not always coherent. Our findings agree with the works of Lee (16) and Aulton (41). For MCC and lactose compacts obtained under 120 MPa, it was reported that the Vickers hardness on the side surface was similar to that on the top surface (16). In reference (41), all tablet surfaces adjacent to the moving punch, were harder than those next to the stationary punch, and the tablets were harder at the centre of the faces. The difference was important for MCC compacts and lower for aCP compacts. Finally, Mullarney (14) reported existence of some anisotropy between the top and side faces, which was higher for aCP compacts than for MCC (the corresponding anisotropy parameters were, respectively, 0.81 and 1.13 for compacts with a solid fraction of 0.85 and 0.64). Aulton (41) as well as Mullarney and Hancock (14) observed variability on the data, which was linked to a consequence of using a point testing method on heterogeneous surface. For example, in reference (14), the authors concluded that it was impossible to discriminate between the top and bottom surface hardness because of the insensitivity of the technique to small difference. A second reason for these different conclusions was the use of different test methods (Vickers hardness and dynamic indentation) and various compact geometries (cylindrical tablets and cubic compacts).

Then, from the analysis of variance (Table VI), the effect of loading direction was not existent on Young's modulus and tensile strength of the tested compacts. Concerning the Brinell hardness, only MCC compacts were affected with a lower hardness for the bottom face.

CONCLUSION

We proposed a simple method to analyse the mechanical property anisotropy of pharmaceutical compacts. This method had the advantage to be valid in the four testing directions (*a*, *b*, *c* and *d* faces) without difficulties in interpreting the experimental results. Concurrently to mechanical test, PGSTE-NMR measurements were performed. It is an innovative approach which is interested in the link between the porous structure and the mechanical property anisotropy. The PGSTE-NMR technique showed that the pore space of MCC compacts was anisotropic, whereas those of aCP compacts were isotropic. Then, the porous structure was connected with the material compaction behaviour under pressure. But this anisotropy did not induce a mechanical property anisotropy, even if these two concepts were assimilated to each other in the literature, which led to some important confusion. The Brinell hardness must be separately considered since it is a local characterization. Some differences were only observed in the axial direction for MCC compacts.

This work was a first step in the study of mechanical property anisotropy of pharmaceutical compacts in relation with their porous structure. A continuation of this work should be the use of a non-destructive contact ultrasonic method in comparison of flexure testing.

ACKNOWLEGEMENTS

The DSX100 Bruker NMR spectrometer and the Micro5 Bruker microimaging probehead used for this study were purchased with grants from CNRS and the Région Centre (France).

REFERENCES

1. Train D. An investigation into the compaction of powders. J Pharm Pharmacol. 1956;8:745–61.
2. Nebgen G, Gross D, Lehmann V, Muller F. H-NMR microscopy tablets. J Pharm Sci. 1995;84:283–91.
3. Djemai A, Sinka IC. NMR imaging of density distributions in tablets. Int J Pharm. 2006;319:55–62.
4. Sinka IC, Burch SF, Tweed JH, Cunningham JC. Measurement of density variations in tablets using X-ray computed tomography. Int J Pharm. 2004;271:215–24.
5. Sinka IC, Motazedian F, Cocks ACF, Pitt KG. The effect of processing parameters on pharmaceutical tablet properties. Powder Tech. 2009;189:276–84.
6. Busignies V, Leclerc B, Porion P, Evesque P, Couarraze G, Tchoreloff P. Quantitative measurements of localized density variations in cylindrical tablets using X-ray microtomography. Eur J Pharm Biopharm. 2006;64:38–50.
7. Zeitler JA, Gladden LF. *In-vitro* tomography and non-destructive imaging at depth of pharmaceutical solid dosage forms. Eur J Pharm Biopharm. 2009;71:2–22.

8. Wu YS, van Vliet LJ, Frijlink HW, Stokroos I, Van der Voort Maarschalk K. Pore direction in relation to anisotropy of mechanical strength in a cubic starch compact. AAPS PharmSciTech. 2008;9:528–35.
9. Busignies V, Porion P, Leclerc B, Evesque P, Tchoreloff P. Application of PGSTE-NMR technique to characterize the porous structure of pharmaceutical tablets. Eur J Pharm Biopharm. 2008;69:1160–70.
10. Ryshkewitch E. Compression strength of porous sintered alumina and zirconia. J Am Ceram Soc. 1953;36:65–8.
11. Edge S, Steele DF, Tobyn MJ, Staniforth JN, Chen A. Directional bonding in compacted microcrystalline cellulose. Drug Dev Ind Pharm. 2001;27:613–21.
12. Kachrimanis K, Malamataris S. Compact size and mechanical strength of pharmaceutical diluents. Eur J Pharm Sci. 2005;24:169–77.
13. Galen S, Zavaliangos A. Strength anisotropy in cold compacted ductile and brittle powders. Acta Mater. 2005;53:4801–15.
14. Mullarney MP, Hancock BC. Mechanical property anisotropy of pharmaceutical excipient compacts. Int J Pharm. 2006;314:9–14.
15. Podczeck F. Investigations into the mechanical strength anisotropy of sorbitol instant compacts made by uniaxial compression. Adv Powder Tech. 2007;18:361–79.
16. Lee J. Structural heterogeneity of pharmaceutical compacts probed by micro-indentation. J Mater Sci Mater Med. 2008;19:1981–90.
17. Akseli I, Hancock BC, Cetinkaya C. Non-destructive determination of anisotropic mechanical properties of pharmaceutical solid dosage forms. Int J Pharm. 2009;377:35–44.
18. Kachrimanis K, Malamataris S. "Apparent" Young's elastic modulus and radial recovery for some tableted pharmaceutical excipients. Eur J Pharm Sci. 2004;21:197–207.
19. Callaghan PT. Principle of nuclear magnetic resonance microscopy. Clarenton Press; 1991.
20. Ek R, Gren T, Henriksson U, Nyqvist H, Nyström C, Ödberg L. Prediction of drug release by characterization of the tortuosity in porous cellulose beads using a spin echo NMR technique. Int J Pharm. 1995;124:9–18.
21. Watson AT, Chang CTP. Characterizing porous media with NMR methods. Prog Nucl Magn Reson Spectrosc. 1997;31:343–86.
22. Porion P, Al-Mukhtar M, Faugère AM, Delville A. ^{23}Na Nuclear Magnetic Resonance and ^{1}H Pulsed Gradient Spin-Echo detection of the critical concentration corresponding to the Isotrope/Nematic transition within aqueous dispersions of charged anisotropic nanoparticles. J Phys Chem B. 2004;108:10825–31.
23. Porion P, Faugère AM, Delville A. ^{1}H and ^{7}Li NMR pulsed gradient spin echo measurements and multiscale modeling of the water and ionic mobility within aqueous dispersions of charged anisotropic nanoparticles. J Phys Chem C. 2008;112:11893–900.
24. ASTM Standard C1161-02c (2008) e1. Standard test method for flexural strength of advanced ceramics at ambient temperature. West Conshocken, PA; 2008. doi:10.1520/C1161-02CR08.
25. Holman LE. The compaction behaviour of particulate materials. An elucidation based on percolation theory. Powder Tech. 1991;66:265–80.
26. Tanner JE. Use of the stimulated echo in NMR diffusion studies. J Chem Phys. 1970;52:2523–6.
27. Busignies V, Tchoreloff P, Leclerc B, Hersen C, Keller G, Couarraze G. Compaction of crystallographic forms of pharmaceutical granular lactoses. II. Compacts mechanical properties. Eur J Pharm Biopharm. 2004;58:577–86.
28. Busignies V, Leclerc B, Porion P, Evesque P, Couarraze G, Tchoreloff P. Investigation and modelling approach of the mechanical properties of compacts made with binary mixtures of pharmaceutical excipients. Eur J Pharm Biopharm. 2006;64:51–65.
29. Mc Donald JH. Handbook of biological statistics. 2nd ed. Baltimore: Sparky House; 2009.
30. Callaghan PT, Coy A, Halpin TPJ, MacGowan D, Packer KJ, Zelaya FO. Diffusion in porous systems and the influence of pore morphology in pulsed gradient spin-echo nuclear magnetic resonance studies. J Chem Phys. 1992;97:651–62.
31. Carman PC. Fluid flow through granular beds. Trans Inst Chem Eng. 1937;15:150–66.
32. Latour LL, Mitra PP, Kleinberg RL, Sotak CH. Time-dependent diffusion coefficient of fluids in porous media as a probe of surface-to-volume ratio. J Magn Reson A. 1993;101:342–6.
33. Latour LL, Kleinberg RL, Mitra PP, Sotak CH. Pore-size distributions and tortuosity in heterogeneous porous media. J Magn Reson A. 1995;112:83–91.
34. Kim AS, Chen H. Diffusive tortuosity factor of solid and soft cake layers: a random walk simulation approach. J Membr Sci. 2006;279:129–39.
35. Busignies-Goddin V. Recherche de lois de mélange sur des propriétés mécaniques. Application à des systèmes granulaires d'intérêt pharmaceutique. Editions Universitaires Européennes. Sarrebruck; 2010.
36. Hertzberg RW. Deformation and fracture mechanics of engineering materials. Chap. 8. 4th revised edition. Wiley; 1996.
37. Wu CY, Ruddy O, Bentham AC, Hancock BC, Best SM, Elliott JA. Modelling the mechanical behaviour of pharmaceutical powders during compaction. Powder Technol. 2005;152:107–17.
38. Amorós JL, Cantavella V, Jarque JC, Feliú C. Green strength testing of pressed compacts. An analysis of the different methods. J Eur Ceram Soc. 2008;28:701–10.
39. Fell JT, Newton JM. Determination of tablet strength by the diametral compression test. J Pharm Sci. 1970;59:688–91.
40. Hentschel ML, Page NW. Elastic properties of powders during compaction. Part 2: elastic anisotropy. J Mater Sci. 2007;42:1269–78.
41. Aulton ME. Indentation hardness profiles across the faces of some compressed tablets. Pharm Acta Helv. 1981;56:133–6.